Available online at www.sciencedirect.com
ScienceDirect
Trans. Nonferrous Met. Soc. China 28(2018) 939−945
Transactions of Nonferrous Metals Society of China
www.tnmsc.cn

Microstructure evolution of $Al_{0.6}CoCrFeNi$ high entropy alloy powder prepared by high pressure gas atomization

Shang-cheng ZHOU[1], Peng ZHANG[1], Yun-fei XUE[1,2], Fu-chi WANG[1,2], Lu WANG[1,2], Tang-qing CAO[1], Zhen TAN[3], Bao-yuan CHENG[1], Ben-peng WANG[1]

1. School of Materials Science and Engineering, Beijing Institute of Technology, Beijing 100081, China;
2. National Key Laboratory of Science and Technology on Materials under Shock and Impact, Beijing Institute of Technology, Beijing 100081, China;
3. College of Materials Science and Engineering, Beijing University of Technology, Beijing 100124, China

Received 26 December 2016; accepted 21 July 2017

Abstract: The influence of cooling rate on the microstructure of $Al_{0.6}CoCrFeNi$ high entropy alloy (HEA) powders was investigated. The spherical HEA powders ($D_{50}\approx$78.65 μm) were prepared by high pressure gas atomization. The different cooling rates were achieved by adjusting the powder diameter. Based on the solidification model, the relationship between the cooling rate and the powder diameter was developed. The FCC phase gradually disappears as particle size decreases. Further analysis reveals that the phase structure gradually changes from FCC+BCC dual-phase to a single BCC phase with the increase of the cooling rate. The microstructure evolves from planar crystal to equiaxed grain with the cooling rate increasing from 3.19×10^4 to 1.11×10^6 K/s.
Key words: $Al_{0.6}CoCrFeNi$; high entropy alloy; high pressure gas atomization; spherical powder; microstructure; cooling rate

1 Introduction

Currently, the universal definition of high entropy alloys (HEAs) is an alloy which consists of at least five principal elements ($N\geq5$), and the concentration of each is in the range of 5%−35% (molar fraction). Due to the high entropy of mixing (ΔS_{mix}), simple solid solution structure formed instead of complicated compounds [1−3]. HEAs have unique properties such as good mechanical properties at cryogenic temperature [4], room temperature [5,6], and elevated temperature [7], as well as outstanding oxidation resistance [8]. These excellent properties offer great potential applications for some extreme environmental engineering including nuclear, turbine and aerospace industries.

A high solidification rate usually leads to a reduction of segregation, refinement of secondary phases or intermetallic compounds [9]. In the process of gas atomization, the cooling rate of powder highly depends on the particle size. That is to say, the microstructure of gas-atomized powders may strongly be related to the cooling rate. $Al_xCoCrFeNi$ HEAs were found that the structure of the as-cast alloy seriously depended on the Al content [10]. KAO et al [11] found that it is a FCC structure when $x<0.45$, a BCC structure when $x>0.88$, or a FCC+BCC duplex structure when $0.45<x<0.88$ [11]. Further, the structure is also influenced by cooling rate. $Al_{0.6}CoCrFeNi$ has FCC+BCC duplex structure, and is probably a near-eutectic high entropy alloy [12] which shows promising application prospect [13,14]. In conclusion, $Al_{0.6}CoCrFeNi$ will be a suitable alloy showing the effect of cooling rate on the phase and microstructure.

High pressure gas atomization is widely used in the preparation of powders for 3D printing. Although HEAs exhibit several excellent properties as we discuss before, only very few works have been reported about the combination of HEAs and 3D printing [15]. We will focus on the property of HEA powders for 3D printing, trying to prove the practicability of gas atomization preparing HEA powders, showing the potential prospect of HEAs applied in 3D printing. Then, $Al_{0.6}CoCrFeNi$ alloy and the gas atomization preparation method were chosen to reveal the relationship between cooling rate and phase structure of the powders.

Foundation item: Project (51471035) supported by the National Natural Science Foundation of China
Corresponding author: Yun-fei XUE; Tel: +86-10-68912709-107; E-mail: xueyunfei@bit.edu.cn
DOI: 10.1016/S1003-6326(18)64728-4

2 Experimental

Alloy ingots with a nominal composition of $Al_{0.6}CoCrFeNi$ were prepared by arc-melting a mixture of pure metals (purity >99.9%, mass fraction). The ingots were repeatedly melted at least four times to ensure chemical homogeneity. Powders of the alloy were produced by high pressure gas atomization. The ingots were re-melted at 1803 K in an induction crucible. The liquid metal is delivered to the tip of the atomization nozzle via a central 4 mm-diameter bore. In order to prevent oxidation of the liquid metal, argon was used as the atomizing gas. The atomization pressure was 9 MPa. Finally, the powders were collected and sieved into six size ranges for further analysis: >150, 75−150, 50−75, 38−50, 30−38 and <30 μm.

X-ray diffraction (XRD) with RIGAKU RINT−2500 X-ray diffractometer was performed using Cu K_α radiation. The powders were first embedded and then the sample was mechanically polished and etched using 0.5 g $CuCl_2$ + 10 mL HCl + 20 mL H_2O. The surface and cross-sectional microstructure was examined using optical microscopy (OM) and JEOL JSM−5400 scanning electron microscope (SEM) operating at 15 kV.

3 Results and discussion

3.1 Size distribution

Figure 1(a) shows the size differential distribution of the powders and Fig. 1(b) shows the cumulative distribution of the powders. The mass percentage of the powder with size of 75−150 μm is more than 40%. The median diameter (D_{50}) of powders is 78.65 μm.

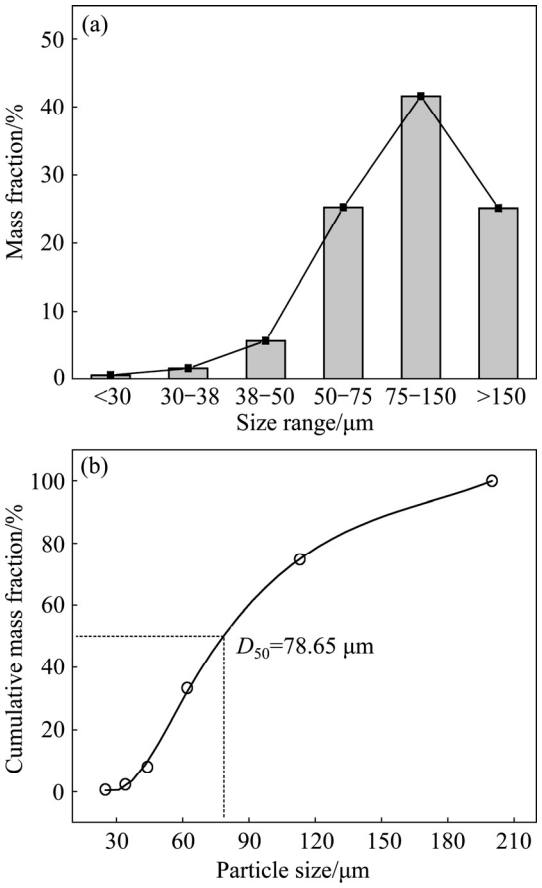

Fig. 1 Differential (a) and cumulative (b) particle size distribution of $Al_{0.6}CoCrFeNi$ HEA powders

3.2 Phase structure

Figure 2 shows the X-ray diffraction patterns of the powders with different sizes. The powder consists of FCC+BCC duplex structure when the particle size is larger than 75 μm. Moreover, the diffraction peak intensity of the FCC phase gradually weakens with a decrease in the particle size. When the particle size is below 75 μm, only a BCC structure exists in the powders.

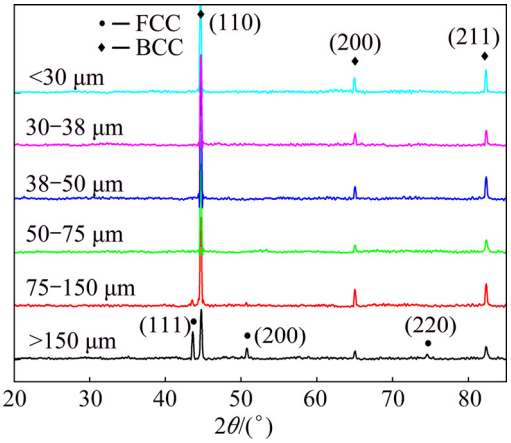

Fig. 2 XRD patterns of $Al_{0.6}CoCrFeNi$ HEA powders with different sizes

3.3 Microstructure

Figure 3 shows the surface morphologies of the powders with different sizes. There are some satellite particles attached on the surface of larger particles, as shown in Figs. 3(a) and (b), which are induced by the droplets flying in argon atmosphere. Larger particles need more time to solidify than finer ones. Thus, solidified finer powder particles are possible to stick to the surface of larger particles. Figure 4 shows the surface microstructure of powders with different diameters. Irregular granular structure is observed on the surface of the powder with a diameter greater than 150 μm. As the particle diameter decreases, irregular granular structure gradually transforms into dendrites, and finally into equiaxed-type microstructures, as shown in Figs. 4(c)−(f). The powder surface becomes gradually smoother with the decrement of particle size.

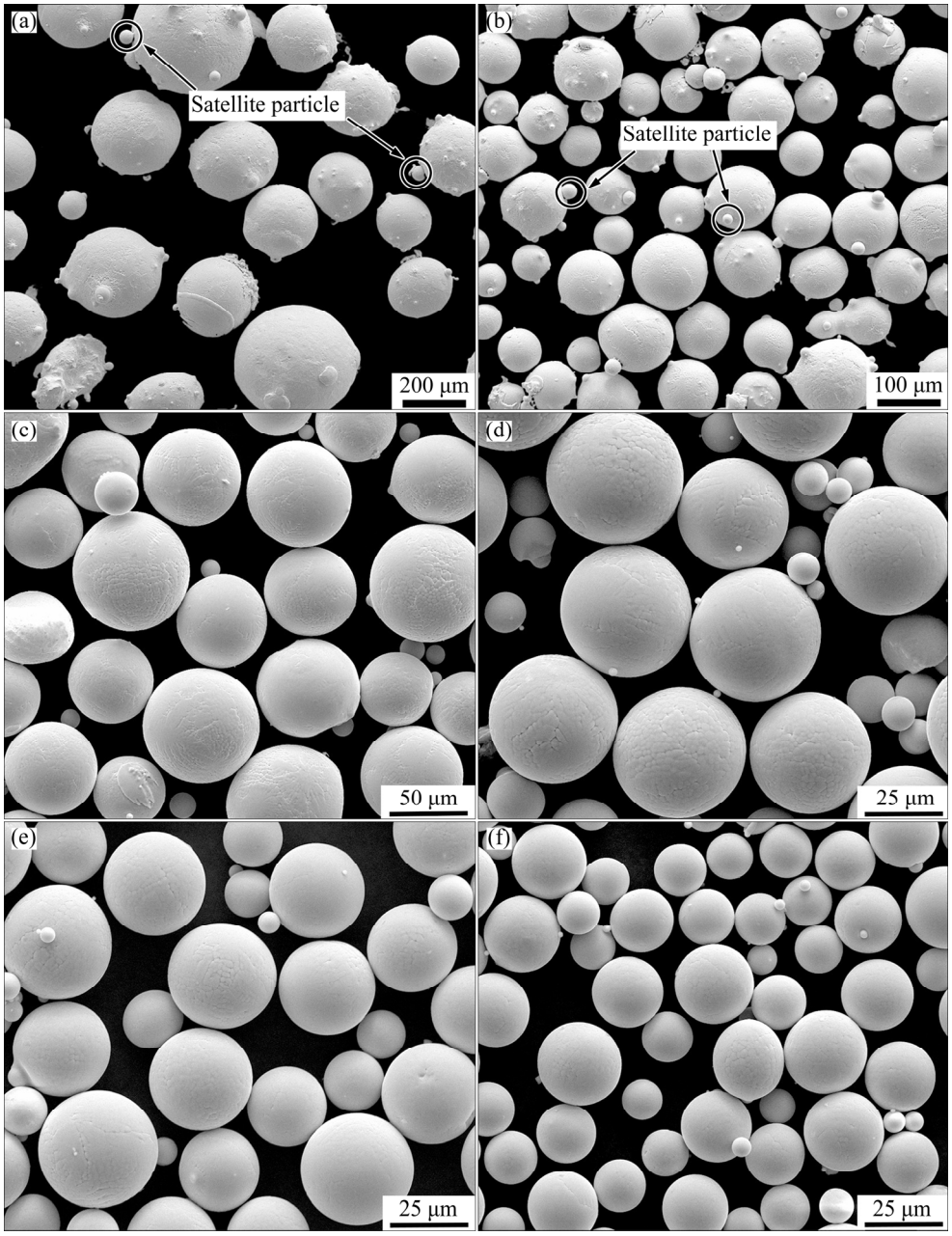

Fig. 3 Surface morphologies of powders with different diameters: (a) >150 μm; (b) 75−150 μm; (c) 50−75 μm; (d) 38−50 μm; (e) 30−38 μm; (f) <30 μm

Figure 5 shows the cross-sectional microstructures of the powders. Planar crystal forms when the particles diameters are above 150 μm. As the particle diameter decreases, the grain gradually transforms from planar crystal into dendrites, cellular crystal, and equiaxed-type microstructure orderly.

3.4 Cooling rate of HEA droplets

The cooling rate of gas atomized HEA powders in the present work is estimated by theoretical models. The model of cooling rate is based on the balance of heat fluxes for a given droplet [16], which can be expressed as

$$c_{pl}\frac{\mathrm{d}T_\mathrm{p}}{\mathrm{d}t}=\frac{6h}{\rho_\mathrm{p}d_\mathrm{p}}(T_\mathrm{p}-T_\mathrm{g})-\frac{6\varepsilon\sigma_\mathrm{b}}{\rho_\mathrm{p}d_\mathrm{p}}(T_\mathrm{p}^4-T_\mathrm{R}^4) \quad (1)$$

During the gas atomization, there exist two ways of heat-transfer during the solidification of droplets: heat radiation and heat convection. It is generally considered that convective heat-transfer is the dominant way. In the case of ignoring the radiation term, the cooling rate of droplets can be expressed as

$$c_{pl}\frac{\mathrm{d}T_\mathrm{p}}{\mathrm{d}t}=\frac{6h}{\rho_\mathrm{p}d_\mathrm{p}}(T_\mathrm{p}-T_\mathrm{g}) \quad (2)$$

where c_{pl} is the specific heat capacity of liquid droplet

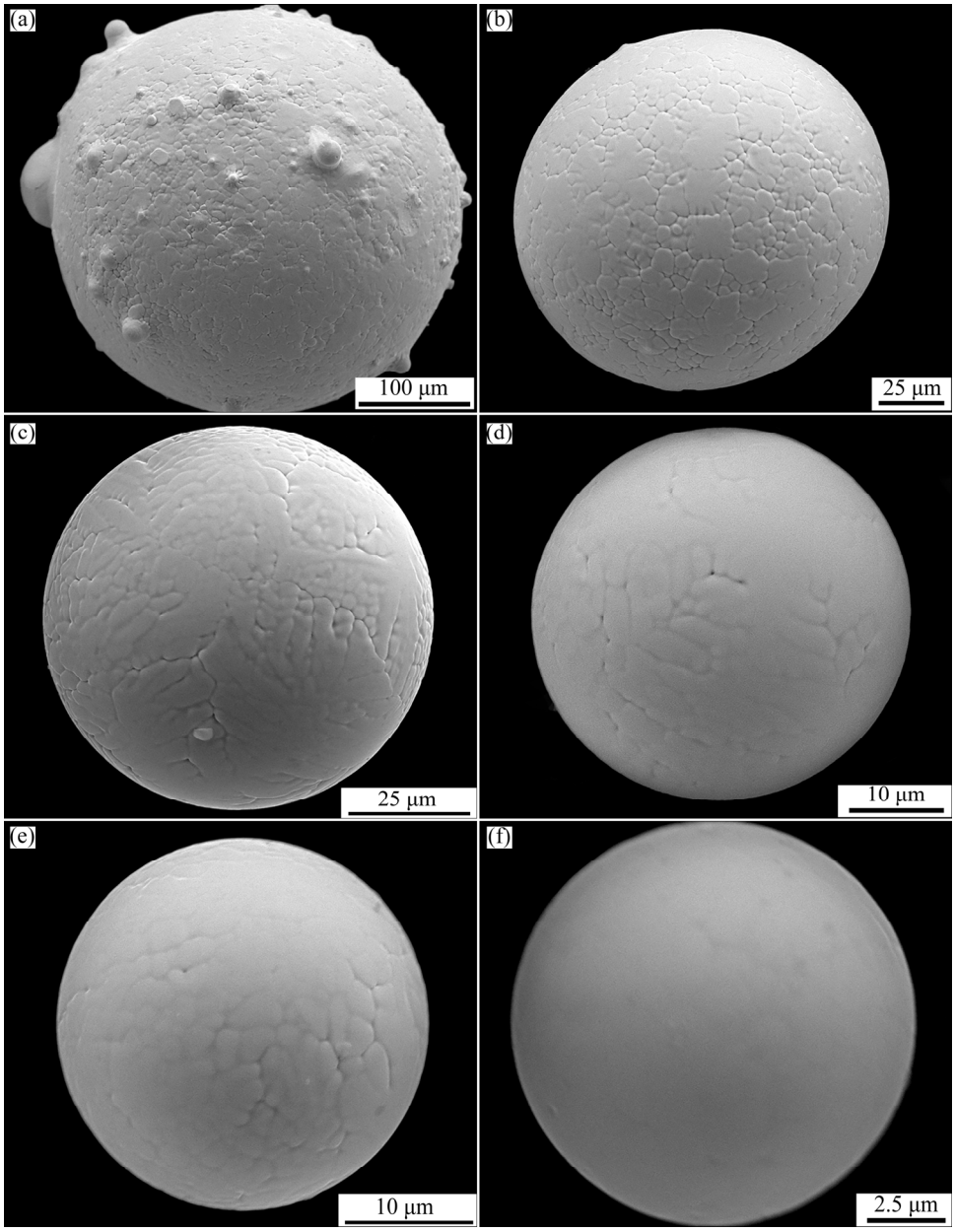

Fig. 4 Microstructures of powders with different diameters on surface: (a) >150 μm; (b) 75−150 μm; (c) 50−75 μm; (d) 38−50 μm; (e) 30−38 μm; (f) <30 μm

material, T_p is the droplet temperature, h is the heat transfer coefficient, ρ is the droplet density, d_p is the droplet diameter, T_g is the gas temperature, t is the time, σ_b is the Stefan−Boltzman constant, and T_R is the effective radiative temperature of the environment of the particle.

SHUKLA et al [17] put forward an empirical model for the convective heat transfer coefficient, h, given by

$$h=\frac{\kappa_g}{d_p}(2+0.6\sqrt{Re}\sqrt[3]{Pr}) \tag{3}$$

where κ_g is the thermal conductivity of gas, Re is the Reynolds numbers, and Pr is the Prandtl number.

Re and Pr are given by

$$Re=\frac{\rho_g d_p(v_g-v_p)}{\mu_g},\ Pr=\frac{c_{pg}\mu_g}{k_g} \tag{4}$$

where c_{pg} is the specific heat capacity of gas, μ_g is the kinematic viscosity of gas, and (v_g-v_p) is the velocity difference between the particle and the gas. Thermo-physical parameters of argon and $Al_{0.6}CoCrFeNi$ HEA are cited in literatures, as given in Table 1.

Before atomization, the initial temperature (T_p) of the liquid alloy is 1803 K, and (v_g-v_p) is 200 m/s. T_g is the environment temperature, 298 K.

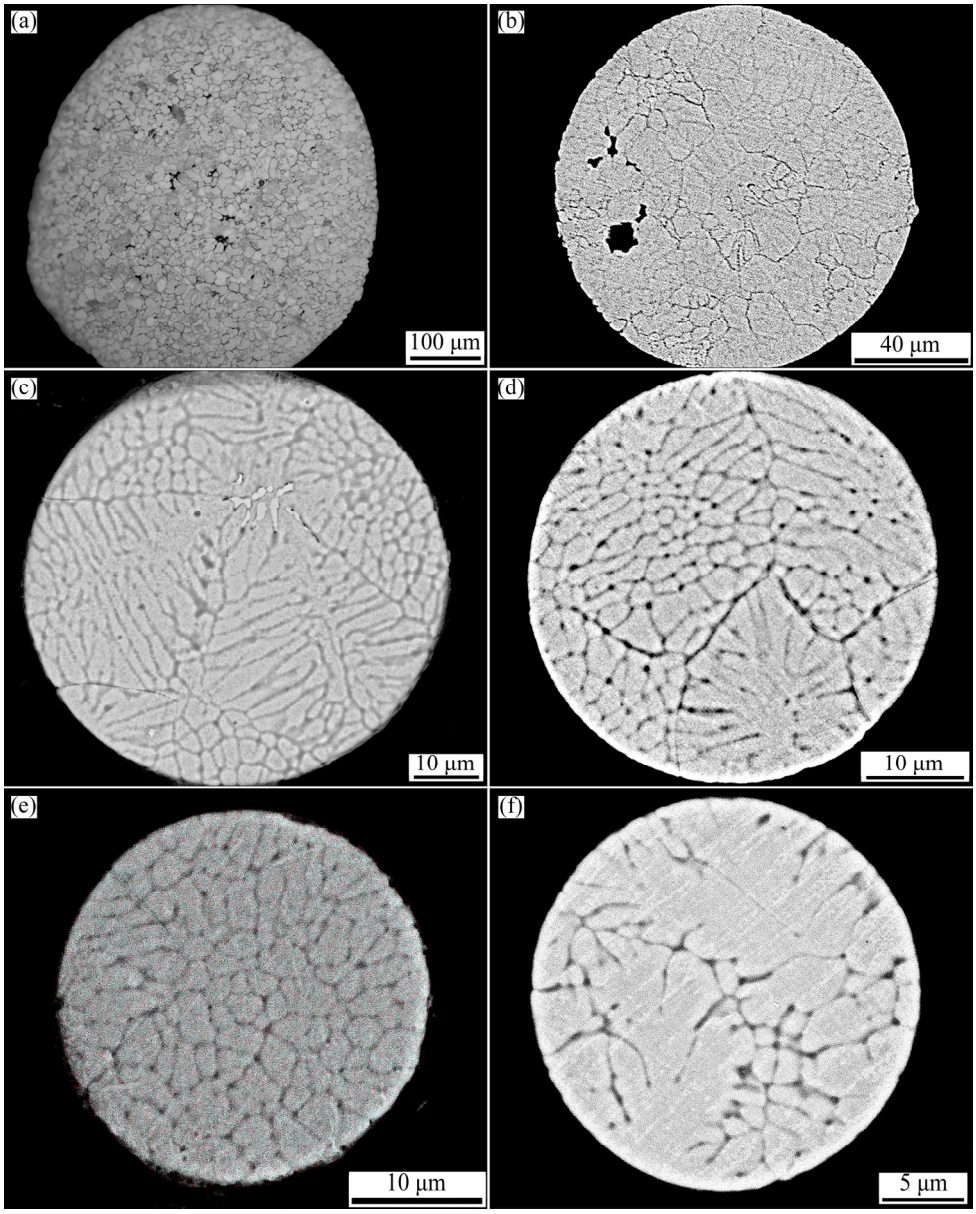

Fig. 5 Cross-sectional morphologies of powders with different diameters: (a) >150 μm; (b) 75−150 μm; (c) 50−75 μm; (d) 38−50 μm; (e) 30−38 μm; (f) <30 μm

Table 1 Thermo-physical parameters of argon and $Al_{0.6}CoCrFeNi$ high entropy alloy

Material	Parameter	Value
Argon	Specific heat capacity, c_{pg}/(J·kg^{-1}·K^{-1})	520
	Density, ρ_g/(kg·m^{-3})	1.654
	Kinematic viscosity, μ/(Pa·s)	22.442×10^{-7}
	Thermal conductivity, κ_g/(W·K^{-1}·m^{-1})	0.01795
High entropy alloy	Specific heat capacity (liquid), c_{pl}/(J·kg^{-1}·K^{-1})	800
	Density, ρ_s/(kg·m^{-3})	7500

According to Eqs. (2)−(4) and Table 1, the cooling rate of droplets as a function of droplet diameter is shown in Fig. 6. When the diameter of droplets is in the range of 20−200 μm, the corresponding cooling rate is calculated to be 1.11×10^6−3.19×10^4 K/s. The cooling rate increases as the droplet diameter decreases. The cooling rate increases sharply when the droplet diameter is below 30 μm. However, when the droplet diameter is above 95 μm, the change trend of cooling rate turns to be gentle.

3.5 Influence of cooling rate on phase structure

According to the calculation results (Fig. 6), the solidification characteristics of $Al_{0.6}CoCrFeNi$ HEA powder are typical of rapid solidification. The process of solidification is deviated from equilibrium. The deviating degree from the equilibrium increases as the cooling rate goes up, which leads to the formation of metastable phase in multiphase systems.

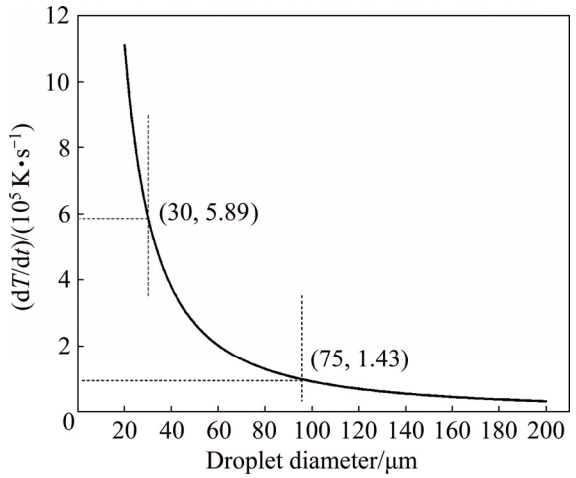

Fig. 6 Calculated cooling rate of droplets as function of droplet diameter

ZHANG et al [12] calculated the isopleth of the Al_xCoCrFeNi alloys with x=0−3 using current thermodynamic description, as shown in Fig. 7. It shows the vertical section of the Al_xCoCrFeNi as a function of x. The phase stability changes when adding Al to the CoCrFeNi alloy. The sequence of phase formation is L→L+FCC→L+FCC+B2→FCC+B2 in the case of equilibrium solidification. According to Fig. 7, the phase structure of the present $Al_{0.6}$CoCrFeNi HEA should be a FCC+BCC mixed structure at room temperature. However, the solidification process would deviate from the equilibrium and enter into the eutectic regions during rapid solidification. The rest of liquid phase would generate eutectic during solidification. The phase structure changes to be FCC+A2+B2. Because the phase content of FCC in eutectic region is less than that in hypoeutectic region, the diffraction peak intensity of FCC gradually weakens (Fig. 2).

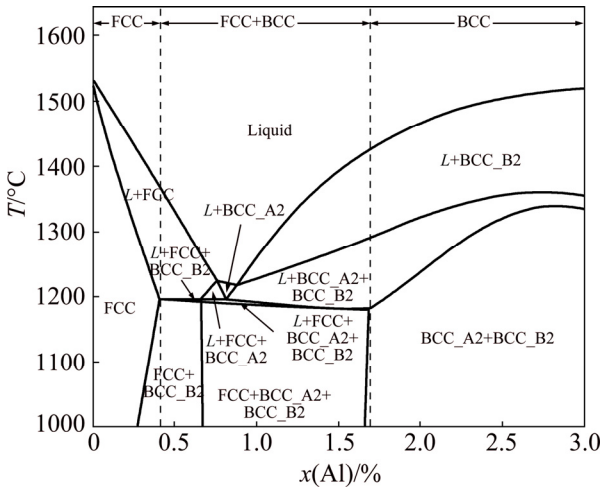

Fig. 7 Calculated isopleth of Al_xCoCrFeNi HEAs with x=0−3 using current thermodynamic description [12]

When the particle size is less than 75 μm and cooling rate is up to 1.43×10^5 K/s, the FCC structure disappears and only a BCC structure is observed. This is mainly induced by the fact that the eutectic process is inhibited due to high cooling rate. On one hand, there is rather narrow temperature range for the eutectic reaction. What we should mention in Fig. 7 is that the temperature only drops by less than 14 °C (1189−1175 °C) for the residual liquid phase to finish eutectic solidification (L→FCC+A2+B2) in the eutectic region. On the other hand, high cooling rate increases the solubility limit of Al in CoCrFeNi, and the amount of the residual liquid phase for L→FCC+A2+B2 reaction in the eutectic region becomes smaller. Both the factors mentioned above make it difficult to form the FCC phase at a high cooling rate.

The formation of planar crystal in Figs. 5(a) and (b) is mainly due to the eutectic reaction, and a straight interface is maintained in front of the solid/liquid interface. Once the eutectic process is inhibited with the increase of cooling rate, the growth pattern of straight interface would be broken and then transforms into dendrite, cellular crystal, equiaxed grain or featureless crystal, as shown in Figs. 5(c)−(f).

4 Conclusions

1) $Al_{0.6}$CoCrFeNi high entropy alloy powders were prepared by high pressure gas atomization. The powders are mainly spherical in shape, and the mean diameter (D_{50}) is 78.65 μm.

2) The FCC phase gradually decreases and disappears as the particle size decreases. This may be the result of higher solubility of Al in CoCrFeNi under high cooling rate, as well as the result of the deviated solidification process from equilibrium.

3) The surface of the powder particles becomes gradually smooth as the diameter decreases. With the decrease of particle size, planar crystal, dendrite, cellular crystal, equiaxed grain and featureless crystal become the dominant microstructure of $Al_{0.6}$CoCrFeNi powders successively. This may be attributed to the inhibited eutectic process brought by increasing cooling rate.

References

[1] TSAI M, YEH J. High-entropy alloys: A critical review [J]. Materials Research Letters, 2014, 2: 107−123.

[2] ZHANG L S, MA G L, FU L C, TIAN J Y. Recent progress in high-entropy alloys [J]. Advanced Materials Research, 2013, 631−632: 227−232.

[3] JIANG L, LU Y P, JIANG H, WANG T M, WEI B N. Formation rules of single phase solid solution in high entropy alloys [J]. Materials Science and Technology, 2016, 32(6): 588−592.

[4] GLUDOVATZ B, HOHENWARTER A, CATOOR D, CHANG E H, GEORGE E P, RITCHIE R O. A fracture-resistant high-entropy

alloy for cryogenic applications [J]. Science, 2014, 345: 1153−1158.
[5] DONG Y, GAO X, LU Y, WANG T, LI T. A multi-component AlCrFe2Ni2 alloy with excellent mechanical properties [J]. Materials Letters, 2016, 169: 62−64.
[6] CHEN Q, LU Y, DONG Y, WANG T, LI T. Effect of minor B addition on microstructure and properties of AlCoCrFeNi multi-component alloy [J]. Transactions of Nonferrous Metals Society of China, 2015, 25: 2958−2964.
[7] WU Y D, CAI Y H, WANG T, SI J J, ZHU J, WANG Y D, HUI X D. A refractory Hf−25−Nb−25−TiV25−Zr−25 high-entropy alloy with excellent structural stability and tensile properties [J]. Materials Letters, 2014, 130: 277−280.
[8] LIU Y, CHENG C, SHANG J, WANG R, LI P, ZHAO J. Oxidation behavior of high-entropy alloys Al*x*CoCrFeNi (*x*=0.15, 0.4) in supercritical water and comparison with HR3C steel [J]. Transactions of Nonferrous Metals Society of China, 2015, 25: 1341−1351.
[9] CAI Z, ZHANG C, WANG R, PENG C, QIU K, WANG N. Effect of pre-annealing on microstructure and compactibility of gas-atomized Al−Si alloy powders [J]. Transactions of Nonferrous Metals Society of China, 2016, 26: 2355−2362.
[10] WANG W, WANG W, WANG S, TSAI Y, LAI C, YEH J. Effects of Al addition on the microstructure and mechanical property of Al*x*CoCrFeNi high-entropy alloys [J]. Intermetallics, 2012, 26: 44−51.
[11] KAO Y, CHEN S, CHEN T, CHU P, YEH J, LIN S. Electrical, magnetic, and Hall properties of Al*x*CoCrFeNi high-entropy alloys [J]. Journal of Alloys and Compounds, 2011, 509: 1607−1614.
[12] ZHANG C, ZHANG F, CHEN S, CAO W. Computational thermodynamics aided high-entropy alloy design [J]. JOM, 2012, 64: 839−845.
[13] LU Y, DONG Y, GUO S, JIANG L, KANG H, WANG T, WEN B, WANG Z, JIE J, CAO Z, RUAN H, LI T. A promising new class of high-temperature alloys: Eutectic high-entropy alloys [J]. Scientific Reports, 2014, 4: 6200.
[14] LU Y, GAO X, JIANG L, CHEN Z, WANG T, JIE J, KANG H, ZHANG Y, GUO S, RUAN H, ZHAO Y, CAO Z, LI T. Directly cast bulk eutectic and near-eutectic high entropy alloys with balanced strength and ductility in a wide temperature range [J]. Acta Materialia, 2017, 124: 143−150.
[15] CHUANG M, TSAI M, WANG W, LIN S, YEH J. Microstructure and wear behavior of Al*x*Co1.5CrFeNi1.5Ti high-entropy alloys [J]. Acta Materialia, 2011, 59: 6308−6317.
[16] MULLIS A M, FARRELL L, COCHRANE R F, ADKINS N J. Estimation of cooling rates during close-coupled gas atomization using secondary dendrite arm spacing measurement [J]. Metallurgical and Materials Transactions B, 2013, 44: 992−999.
[17] SHUKLA P, MANDAL R K, OJHA S N. Non-equilibrium solidification of undercooled droplets during atomization process [J]. Bulletin of Materials Science, 2001, 24: 547−554.

气雾化制备 $Al_{0.6}CoCrFeNi$ 高熵合金粉体的显微组织演变

周上程[1]，张 鹏[1]，薛云飞[1,2]，王富耻[1,2]，王 鲁[1,2]，曹堂清[1]，谈 震[3]，程宝元[1]，王本鹏[1]

1. 北京理工大学 材料学院，北京 100081；
2. 北京理工大学 冲击环境材料技术国家重点实验室，北京 100081；
3. 北京工业大学 材料科学与工程学院，北京 100124

摘 要：研究冷却速率对 $Al_{0.6}CoCrFeNi$ 高熵合金粉体的影响。使用高压气雾化法制备 $Al_{0.6}CoCrFeNi$ 球形高熵合金粉体，通过调整粉体粒径可以获得不同的冷却速率。基于凝固模型计算，获得冷却速率和粉体直径之间的关系。结果表明，随着粉体粒径的减小，粉体中 FCC 相的含量逐渐减小；进一步分析可以发现，随着冷速的增加，粉体由 FCC+BCC 双相结构逐渐转变为 BCC 单相结构；随着冷速从 3.19×10^4 K/s 增至 1.11×10^6 K/s，粉体的显微组织表现出从平面晶到等轴晶的转变。

关键词：$Al_{0.6}CoCrFeNi$；高熵合金；高压气雾化；球形粉体；显微组织；冷却速率

(Edited by Bing YANG)